The prodrug of 7,8-dihydroxyflavone development and therapeutic efficacy for treating Alzheimer's disease

Chun Chen[a,b], Zhihao Wang[b], Zhentao Zhang[b], Xia Liu[b], Seong Su Kang[b], Ying Zhang[a], and Keqiang Ye[a,b,1]

[a]College of Biosystems Engineering and Food Science, Zhejiang University, Zhejiang 310058, China; and [b]Department of Pathology and Laboratory Medicine, Emory University School of Medicine, Atlanta, GA 30322

Edited by Solomon H. Snyder, Johns Hopkins University School of Medicine, Baltimore, MD, and approved December 12, 2017 (received for review October 27, 2017)

The BDNF mimetic compound 7,8-dihydroxyflavone (7,8-DHF), a potent small molecular TrkB agonist, displays prominent therapeutic efficacy against Alzheimer's disease (AD). However, 7,8-DHF has only modest oral bioavailability and a moderate pharmacokinetic (PK) profile. To alleviate these preclinical obstacles, we used a prodrug strategy for elevating 7,8-DHF oral bioavailability and brain exposure, and found that the optimal prodrug R13 has favorable properties and dose-dependently reverses the cognitive defects in an AD mouse model. We synthesized a large number of 7,8-DHF derivatives via ester or carbamate group modification on the catechol ring in the parent compound. Using in vitro absorption, distribution, metabolism, and excretion assays, combined with in vivo PK studies, we identified a prodrug, R13, that prominently up-regulates 7,8-DHF PK profiles. Chronic oral administration of R13 activated TrkB signaling and prevented Aβ deposition in 5XFAD AD mice, inhibiting the pathological cleavage of APP and Tau by AEP. Moreover, R13 inhibited the loss of hippocampal synapses and ameliorated memory deficits in a dose-dependent manner. These results suggest that the prodrug R13 is an optimal therapeutic agent for treating AD.

7,8-dihydroxyflavone | prodrug | pharmacokinetics | TrkB | Alzheimer's disease

Alzheimer's disease (AD), the leading cause of dementia worldwide, is characterized by accumulation of β-amyloid peptide (Aβ) within the brain, along with hyperphosphorylated and cleaved forms of the microtubule-associated protein Tau. At present, drugs used for the treatment of AD only slightly delay the inevitable symptomatic progression of the disease and do not affect the main neuropathological hallmarks of the disease, i.e., senile plaques and neurofibrillary tangles. Reduced acetylcholine neurotransmission due to loss of neurons in the basal forebrain and depletion of choline acetyltransferase is observed in AD pathology (1).

Currently, there are two types of medications to treat AD: cholinesterase inhibitors and *N*-methyl-D-aspartate receptor (NMDAR) antagonists. The first category of inhibitors blocks the activity of acetylcholinesterase, thereby increasing acetylcholine levels in the CNS to restore cognitive functions. The second category inhibits overactivation of NMDA-induced glutamate excitotoxicity. These drugs can only partially alleviate the symptoms of AD (2).

The amyloid hypothesis has historically dominated the proposed pathology of AD. However, over the last decade, efforts to target the traditional pathways have been consistently ineffective (3). Therefore, it is of urgent need to develop more potent agents to manage cognitive impairment and disease-modifying agents that prevent or delay the onset of AD.

Neurotrophins are growth factors that regulate neuronal development, differentiation, and survival. Neurotrophins consist of four related proteins: nerve growth factor (NGF), brain-derived neurotrophic factor (BDNF), neurotrophin-3 (NT-3), and neurotrophin-4 (NT-4/5). Neurotrophins exert the trophic effects via the cognate Trk receptors. It has been well documented that BDNF expression is reduced in the brains of patients with AD (4). BDNF exerts a protective role against AD pathogenesis, and has been shown to increase learning and memory in demented animals (5). BDNF gene delivery has been reported as a novel potential therapy in diverse models related to AD (6). Thus, the preclinical evidence strongly supports that BDNF might be useful as a therapeutic agent for a variety of neurologic disorders. The outcomes of several clinical trials using recombinant BDNF are disappointing, however. Presumably, this is due to poor delivery and the short in vivo half-life of BDNF.

To search for TrkB receptor agonists to mimic BDNF, we used cell-based screening. We found that 7,8-dihydroxyflavone (7,8-DHF) specifically binds to the TrkB receptor extracellular domain and acts as a selective TrkB agonist, which mimics the physiological actions of BDNF (7). Remarkably, systemic administration of 7,8-DHF can activate TrkB receptors in brains and induce BDNF-like behavioral phenotypes, such as enhanced learning and memory, and antistress or antidepressant-like effects in rodents in a TrkB-dependent manner (8–10). Recently, several independent studies have shown that 7,8-DHF rescues memory deficits in different AD animal models, restoring deficient TrkB signaling without affecting endogenous BDNF levels. Interestingly, 7,8-DHF represses BACE1 expression and lowers levels of Aβ40 and Aβ42. Strikingly, it improves spatial memory and increases thin spine density in a mouse model of AD-like neuronal loss. Therefore, 7,8-DHF represents a novel oral bioactive therapeutic agent for treating AD (11–14). Taken together, these studies indicate that 7,8-DHF displays prominent therapeutic efficacy toward AD through its action as a TrkB receptor agonist.

Dozens of independent studies have shown that 7,8-DHF mimics the physiological actions of BDNF in numerous animal models (15–17), and chronic treatment with 7,8-DHF has demonstrated no detectable toxicity (10). Remarkably, 7,8-DHF

Significance

In this study, we used a prodrug strategy to improve the druggability of 7,8-DHF, which mimics the physiological actions of BDNF in a variety of animal models but with modest oral bioavailability, by improving its PK profiles. In 5XFAD mouse model, we demonstrate that the optimal prodrug R13 increases the half-life, oral bioavailability, and brain exposure of 7,8-DHF. Most importantly, R13 robustly displays promising therapeutic efficacy by strongly activating TrkB and repressing AEP, which plays a crucial role in the pathogenesis of Alzheimer's disease (AD), leading to elimination of senile plaques in the AD mouse brain.

Author contributions: C.C., X.L., and K.Y. designed research; C.C. and Z.W. performed research; C.C., Z.Z., X.L., S.S.K., Y.Z., and K.Y. contributed new reagents/analytic tools; C.C. and K.Y. analyzed data; and C.C. and K.Y. wrote the paper.

The authors declare no conflict of interest.

This article is a PNAS Direct Submission.

[1]To whom correspondence should be addressed. Email: kye@emory.edu.

This article contains supporting information online at www.pnas.org/lookup/suppl/doi:10.1073/pnas.1718683115/-/DCSupplemental.

penetrates the blood-brain barrier (BBB) and is orally bioactive (18). A structure-activity relationship study showed that the catechol moiety in 7,8-DHF is critical for its agonistic effect (10), and that this compound has suboptimal oral bioavailability and brain exposure (18). Taken together, these findings support that 7,8-DHF is efficacious and safe for treating AD chronically and orally.

Given 7,8-DHF's favorable safety and remarkable efficacy in treating various neurologic diseases, including AD, we believe that the prodrug strategy to improve its oral bioavailability and exposure in circulation system should be an ideal approach. Our metabolism study showed that the catechol group is extensively conjugated by glucuronidation, sulfation, and methylation in the liver, leading to the poor oral bioavailability (18). In the present study, we synthesized dozens of derivatives to modify the catechol group; monitored the prodrugs' intestine microsomal stability, liver microsomal stability, and plasma stability; and examined some of the favorable compounds' chemical stability and Caco-2 permeability. We found that prodrug R13 exhibited good absorption and was readily hydrolyzed into 7,8-DHF in liver microsomes. Notably, R13 has a very long half-life, and it improves 7,8-DHF's oral bioavailability from 4.6% to ∼10.5%. The plasma concentration and brain exposure are also significantly enhanced. In a 5XFAD mice strain, chronic oral administration of R13 alleviated Aβ deposition, attenuated the loss of hippocampal synapse, and ameliorated memory deficits in a dose-dependent manner. These exciting data provide a groundwork for moving this prodrug into clinical trials.

Results

Synthesizing Prodrugs of 7,8-Dihydroxyflavone via Medicinal Chemistry. 7,8-DHF is orally bioactive and penetrates the BBB (18). Previous studies have shown that 7,8-DHF is safe for chronic treatment and efficacious for treating AD, at least in animal models (11–13). Thus, this compound itself is good enough for preclinical investigation. Its oral bioavailability is not optimal, however. The catechol group makes 7,8-DHF and its lead compounds labile for fast metabolism, including glucuronidation, sulfation, methylation, and so on (18). Since the catechol group is essential for the pharmacophore, we wished to use a prodrug strategy to elevate the bioavailability. To do so, we synthesized numerous esters or carbamates by changing the hydroxy groups on the catechol ring in 7,8-DHF (Fig. 1*A* and *SI Appendix*, Fig. S1). The detailed synthetic routes and characterization of derivatives are described in *Materials and Methods*.

Identifying the Optimal Prodrug with Appropriate in Vitro PK Profiles. To identify the ideal prodrug, we used the strategy outlined in Fig. 1*B*. The compounds should be stable in both aqueous solution and at room temperature for a long shelf life. Moreover, the optimal derivatives should be stable in intestinal microsomes during absorption, but can be hydrolyzed in liver microsomes or plasma into 7,8-DHF. In addition, the prodrugs should exhibit favorable Caco-2 permeability to allow prominent absorption. The derivatives meeting these standards will be subjected to an in vivo PK study in mice, and 7,8-DHF brain exposure will be determined after oral administration of the prodrug.

On intestinal microsome, liver microsome, and plasma stability screening, among the 20 synthetic derivatives, only R5, R7, R13, R16, R17, and R18 were relatively stable in intestinal microsomes and hydrolyzable in both liver microsomes and plasma. Unfortunately, R7 barely yielded free 7,8-DHF in human liver microsomes, and R16 or R17 failed to release any detectable 7,8-DHF, indicating that these two compounds have different hydrolytic chemistries (*SI Appendix*, Tables S1–S3). Although R18 was relatively stable under both conditions and was also hydrolyzed into 7,8-DHF, its Caco-2 permeability (R_e of 61.6) was very poor (*SI Appendix*, Tables S4 and S5). Taken together, the in vitro screening assays support R13 as the sole appropriate candidate for further investigation.

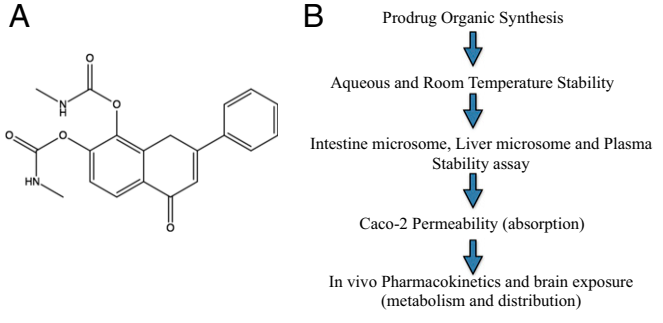

Fig. 1. (*A*) R13: 7,8-DHF prodrug chemical structure. (*B*) In vitro absorption, distribution, metabolism, and excretion screening strategy for prodrugs.

In Vivo PK and Brain Exposure of R13. We tested the in vivo PK/BBB profiles of 7,8-DHF and R13 after dosing R13 in six mice. Three animals in group 1 were dosed orally with 7,8-DHF at 50 mg/kg, and three animals in group 2 were dosed orally with R13 at 36 mg/kg. Blood samples were collected from all animals up to 8 h after dosing. Concentrations of 7,8-DHF in the plasma samples were determined using LC-MS/MS. Pharmacokinetic analysis was performed using a noncompartmental method. Following a single oral administration of R13 at a dose of 36 mg/kg, the mean C_{max} and T_{max} values for 7,8-DHF were 129 ng/mL and 30 min, respectively, and the mean area under the curve (AUC) (0–t) value was 11,880 min ng/mL. The mean value of oral bioavailability for R13 was 10.5%. (*SI Appendix*, Table S6). Notably, 7,8-DHF $T_{1/2}$ released from R13 was 219.6 min versus 134 min by parent compound, indicating the prodrug can sustainably release 7,8-DHF in the circulation system.

For BBB study, plasma samples and the brains were collected from three animals at each designated postdose time point (3, 10, and 30 min and 1, 2, 4, 6, and 8 h). Concentrations of 7,8-DHF and R13 in the plasma samples and brain were determined by LC-MS/MS. The concentration ratio of brain/plasma was calculated, and PK analysis was performed using a noncompartmental method. Following a single oral administration of R13 at a dose of 72.5 mg/kg, the mean C_{max} and T_{max} values for 7,8-DHF were 56 ng/mL and 2 h, respectively, in plasma samples, and 46 ng/mL and 4 h, respectively, in brain samples. In vivo BBB study showed that 7,8-DHF plasma concentrations from prodrug R13 were higher than those from the parent compound (50 mg/kg) on oral administration. Strikingly, 7,8-DHF was detectable in the plasma even at 8 h, indicating the prodrug can sustainably release 7,8-DHF in the circulation system. Notably, the 7,8-DHF concentration from R13 in the brain was >5 ng/g even after 240 min (Fig. 2 *A*–*C*). Overall, this compound has the favorable druggable properties. Of note, R13 readily hydrolyzes into an intermediate T1 under neutral pH, before 7,8-DHF is finally released in vitro, although R13 is very stable under pH 1.2 (Fig. 2*D*). Accordingly, we monitored T1 concentrations in both the plasma and brain on oral administration of different doses of R13. As expected, T1 was significantly elevated in the plasma, but not in the brain, in a dose-dependent manner at 2 h. Its concentrations were much higher than those of 7,8-DHF, supporting the concept that R13 is hydrolyzed into T1 first before it is finally decayed into 7,8-DHF in vivo, in alignment with in vitro observations (Fig. 2*E*).

Oral Administration of R13 Activates TrkB and Downstream Signaling Pathways in Mouse Brain. Given the molecular weights of R13 and 7,8-DHF of 368 and 254, respectively, 7.25, 21.8, and 43.6 mg/kg of R13 are equivalent to 5, 15, and 30 mg/kg of 7,8-DHF,

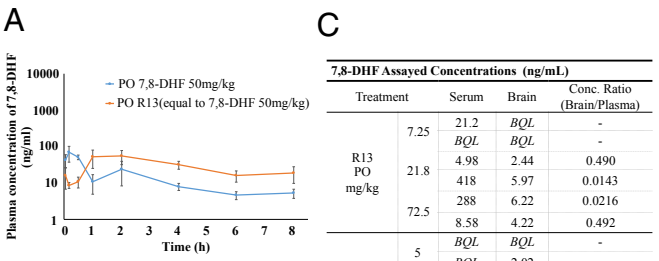

C

7,8-DHF Assayed Concentrations (ng/mL)				
Treatment		Serum	Brain	Conc. Ratio (Brain/Plasma)
R13 PO mg/kg	7.25	21.2	*BQL*	-
		BQL	*BQL*	-
	21.8	4.98	2.44	0.490
		418	5.97	0.0143
	72.5	288	6.22	0.0216
		8.58	4.22	0.492
7,8-DHF PO mg/kg	5	*BQL*	*BQL*	-
		BQL	2.02	-
	15	23.3	*BQL*	-
		8.41	*BQL*	-
	50	22.4	6.92	0.309
		48.9	8.81	0.180
MEAN		84.5	81.1	0.251
STDEV		145	47.8	0.215

Homogenization Dilution factor (1:3) already calculated for brain samples

BQL - *Below Quantitation Limit, < 0.500 ng/mL, for serum*
BQL - Below Quantitation Limit, < 2.00 ng/mL, for brain
- Not Applicable

D

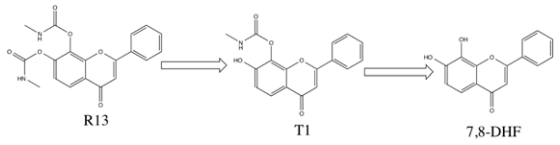

E

R13 Dose level (mg/kg)	7,8-DHF Assayed concentrations						T1 Assayed concentrations					
	Plasma (ng/ml)			Brain (ng/g)			Plasma (ng/ml)			Brain (ng/g)		
		Mean	SD		Mean	SD		Mean	SD		Mean	SD
21.8	2.8	2.1	0.91	*BQL*	-	-	15.5	10.2	4.71	*BQL*	-	-
	1.0			*BQL*			8.8			*BQL*		
	2.4			*BQL*			6.4			*BQL*		
43.6	4.0	4.8	2.01	*BQL*	-	-	33.0	34.0	17.80	*BQL*	-	-
	3.3			*BQL*			16.7			*BQL*		
	7.1			*BQL*			52.2			*BQL*		
72.5	5.4	6.9	4.09	2.7	3.4	1.0	39.1	42.3	22.60	*BQL*	-	-
	3.7			*BQL*			21.4			*BQL*		
	11.5			4.1			66.3			*BQL*		

Fig. 2. 7,8-DHF concentrations in brain and plasma after oral administration of R13. (*A* and *B*) Twenty-four male CD1 mice were given 78 mg/kg of R13 (equal to 7,8-DHF 50 mg/kg), which was dissolved in DMSO and resuspended in 5% DMSO/95% methylcellulose (0.5%, wt/vol). At indicated time points, three mice/group were killed, and serum and brain samples were collected. 7,8-DHF was quantitatively analyzed by LC-MS/MS. Even at 8 h after oral administration, >19 ng/mL of 7,8-DHF was detected in the plasma. 7,8-DHF >8 ng/g was detected in mouse brains at 2 h and persisted for >4 h. (*C*) Six 5XFAD mice were given 7.25 mg/kg, 21.8 mg/kg, and 72.5 mg/kg of R13, and another six 5XFAD mice were given 7,8-DHF at 5 mg/kg, 15 mg/kg, and 50 mg/kg. After 4 h, two mice/group were killed, and serum and brain samples were collected. 7,8-DHF was quantitatively analyzed by LC-MS/MS. (*D*) R13 hydrolysis route. T1 is the major intermediate released from R13 in pH 1.2–7.4 buffer, mimicking the pH change in the transition from stomach to intestine. (*E*) Nine mice were given R13 at doses of 21.8, 43.6, and 72.5 mg/kg. After 4 h of administration, three mice/group were killed, and serum and brains were collected. 7,8-DHF and T1 were quantitatively analyzed by LC-MS/MS.

respectively. To explore whether chronic oral administration of R13 can activate TrkB in mouse brain, we fed 5XFAD mice with R13 or vehicle starting at age 2 mo. After 3 mo of drug treatment, we monitored TrkB activation in mouse brain by immunohistochemistry (IHC) analysis with anti-phosphorylated TrkB (p-TrkB) antibody. Immunoblotting analysis revealed that the TrkB was markedly activated in R13-treated 5XFAD mice. Quantitative analysis revealed that p-TrkB signals, but not total TrkB levels, were notably elevated on R13 treatment (Fig. 3*A*). As expected, TrkB receptors were more prominently phosphorylated in 5XFAD mice treated with R13 than in those treated with vehicle control, as were the downstream AKT and ERK/MAPK pathways. The signals were up-regulated in a dose-dependent manner (Fig. 3*A*). This result was also confirmed in the hippocampus in R13-treated 5XFAD mice by IHC staining with anti–p-TrkB Y816 (Fig. 3*B*).

Given that 7,8-DHF can pass the BBB, these results indicate that chronic oral administration of R13 activates TrkB receptor and its downstream signaling pathways in the brain. At the 21.8 mg/kg dose, R13 robustly provoked TrkB activation in the hippocampus.

Chronic Oral Administration of R13 Prevents Synaptic Loss in 5XFAD Mice. Synaptic loss is believed to be the basis of cognitive impairment in the early phases of AD (19). In 5XFAD model, significant synaptic loss and behavior deficit are detected at 5 mo old, when there is no detectable neuronal loss (20). We first assessed the density of dendritic spines along individual dendrites of pyramidal neurons by Golgi staining. The density of dendritic spines was markedly decreased in the 5XFAD mice model compared with nontransgenic mice. Interestingly, the decreased spine density was noticeably rescued by R13 treatment (Fig. 4 *A* and *B*). Since one dendritic spine can form more than one synapse, we directly quantified the densities of synapses in the CA1 area in the 5XFAD mouse brains by EM. 5XFAD mice showed a significant reduction in synaptic density. R13 treatment significantly reversed the loss of synaptic density in a dose-dependent manner (Fig. 4 *C* and *D*). We further confirmed

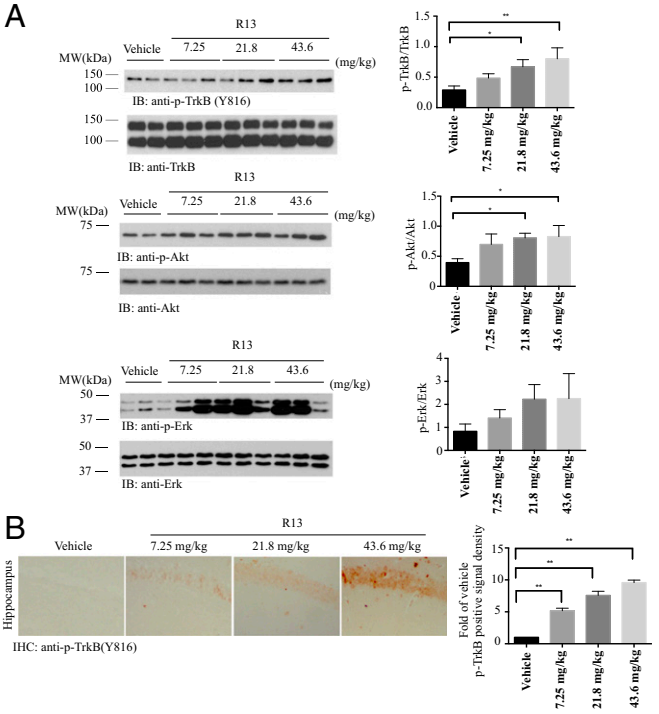

Fig. 3. R13 elicits TrkB and downstream signaling activation in 5XFAD mice. (*A*) R13 activates TrkB signaling cascade in the hippocampus of 5XFAD mice in a dose-dependent manner. R13 was dissolved in pure DMSO, then suspended in 0.5% methylcellulose at final concentration of 5% DMSO/0.5% methylcellulose. The suspension was orally administrated to 2 mo old 5XFAD mice (7.25, 21.8 or 43.6 mg/kg/d) consecutively for 3 mo, and the brain lysates were prepared. The p-TrkB and its downstream signals were monitored by immunoblotting, and the ratio of p-TrkB/TrkB, p-Akt/Akt and p-ERK/ERK were quantitatively analyzed. Data are shown as mean ± SEM. $*P < 0.01$. (*B*) IHC staining of p-TrkB in 5XFAD brain sections. Here 2-mo-old 5XFAD mice were fed with R13 or vehicle consecutively for 3 mo. The phosphorylation of TrkB in dentate gyrus was detected by IHC with anti–p-TrkB 816 antibodies. (Scale bar: 50 μm.) Quantification of p-TrkB$^+$ neurons in the dentate gyrus. Note that R13 treatment elicited the phosphorylation of TrkB in 5XFAD mice. Data are shown as mean ± SEM. $*P < 0.01$.

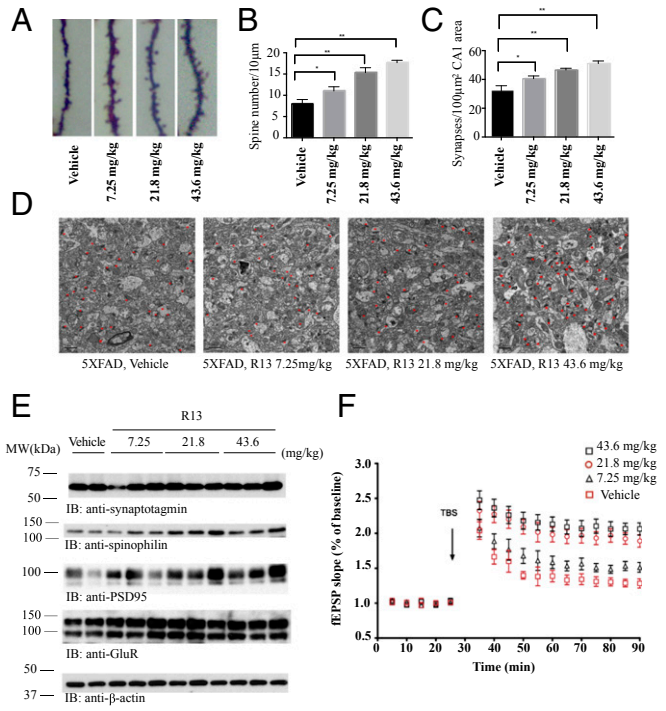

Fig. 4. R13 prevents the synaptic loss in hippocampal CA1 area of 5XFAD mice. (*A*) R13 reversed the synaptic loss in 5XFAD mice. The dendritic spines from apical dendritic layer of the CA1 region were analyzed by Golgi staining. (Scale bar: 5 μm.) (*B*) Quantitative analysis of spine density. The decreased spine density in 5XFAD mice was reversed by R13 in a dose-dependent manner. $n = 6$ in each group. $^*P < 0.01$. (*C*) Quantitative analysis of the synaptic density in vehicle- and R13-treated 5XFAD mice. 5XFAD mice show decreased synaptic density, which was reversed by R13. Data are shown as mean ± SEM. $^*P < 0.01$. (*D*) Representative EM image of the synaptic structures. Red stars indicate the synapses. (Scale bar: 1 μm.) (*E*) Immunoblotting analysis of synaptic markers in brain homogenates from mice treated with vehicle or R13. R13 treatment increased the expression of synaptic markers in 5XFAD mice. (*F*) LTP of field excitatory postsynaptic potentials (fEPSPs) was induced by 3XTBS (theta-burst stimulation) (four pulses at 100 Hz, repeated three times with 200-ms intervals). The traces shown are representative fEPSPs recorded at time points 1 (vehicle-treated 5XFAD mice), 2, 3, and 4 (R13-treated 5XFAD mice). The magnitude of LTP in 5XFAD mice is significantly lower in vehicle-treated transgenic mice, and R13 treatment reversed the LTP impairment. $n = 5$ in each group. Data are presented as mean ± SEM. $^*P < 0.05$, vehicle-treated vs. R13-treated mice.

these findings by immunoblotting using presynaptic markers (synaptotagmin) and postsynaptic markers (GluR1, PSD95, and spinophilin). 5XFAD mice displayed a considerable decrease in these synaptic markers, indicating synaptic degeneration (12). R13 treatment reversed the reduction of synaptic markers (Fig. 4*E*). Electrophysiology analysis demonstrated that R13 increased long-term potentiation in a dose-dependent manner (Fig. 4*F*), in agreement with the findings of augmentation of synapses by R13. These results suggest that activation of the TrkB receptor by R13 inhibits the loss of synapses in 5XFAD mice and improves synaptic plasticity.

R13 Alleviates Aβ Deposition and Rescues Memory Deficits in 5XFAD Mice. We further tested the deposition of Aβ by IHC with anti-Aβ antibody. The dose-dependent Aβ deposition in both brain regions was significantly lower in the R13-treated group than in the control group (Fig. 5 *A*–*C*). We further detected the effect of R13 treatment on senile plaque formation by thioflavin-S staining. 5XFAD mice showed evident plaque deposition in both the cortex and the hippocampus at age 5 mo. Strikingly, the number of plaques and plaque area fraction were significantly decreased in both areas in R13-treated mice compared with vehicle control-treated mice (*SI Appendix*, Fig. S2 *A*–*C*). To verify whether R13 inhibits the production of Aβ, the concentrations of total Aβ42 and Aβ40 were quantitatively determined by ELISA. Interestingly, Aβ40 concentrations in 5XFAD mice brain were decreased by R13 at all doses tested, and although Aβ42 concentrations displayed a trend toward reduction with R13, the differences were not statistically significant (Fig. 5 *D* and *E*). Thus, these results suggest that chronic oral R13 administration may prevent Aβ deposition and Aβ40 production.

The hippocampus-dependent spatial memory of 5XFAD mice was assessed using the Morris water maze test. The average latency (Fig. 5 *F* and *G*) and swim path length (*SI Appendix*, Fig. S2 *D* and *E*) for each of the five acquisition days were calculated and plotted. A two-way mixed ANOVA (group × training day) on latency revealed a main effect of training day ($P < 0.01$) and of group ($P < 0.01$), but not of interaction (Fig. 5*F*). The AUC of latency was greater in vehicle-treated 5XFAD mice compared with nontransgenic control mice, indicating impaired acquisition of the spatial learning task; however, the learning impairment in 5XFAD mice was attenuated by R13 treatment (Fig. 5*G*). A mixed two-way ANOVA on swim path distance also revealed a significant main effect of training day ($P < 0.01$) and of group ($P < 0.01$), but not of interaction (*SI Appendix*, Fig. S2*D*). The AUC of the swim path distance was greater in 5XFAD mice compared with nontransgenic control mice, and was decreased by R13 treatment (*SI Appendix*, Fig. S2*E*). The memory recall for the platform location was assessed in the probe trail when the platform was removed and the mice were allowed to search for

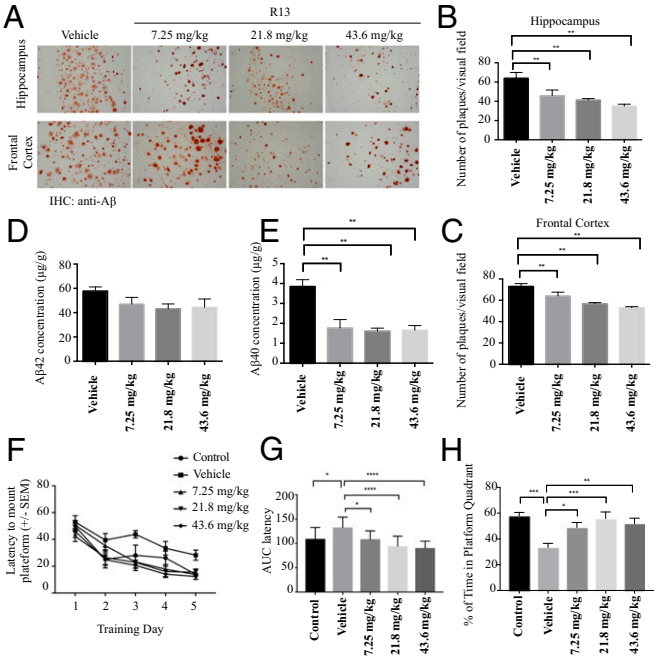

Fig. 5. R13 alleviates Aβ deposition and reduces the concentrations of total Aβ, improving the spatial learning and memory of 5XFAD mice. (*A*) IHC analysis of Aβ deposits in 5XFAD mice. (Scale bar: 100 μm.) (*B* and *C*) Quantitative analysis of amyloid plaques. Amyloid deposition in 5XFAD mice was significantly decreased by orally administrated R13 at all doses. $^*P < 0.01$. (*D* and *E*) Aβ42 and Aβ40 ELISA. R13 significantly reduced the concentrations of Aβ40, but not of Aβ42, in mouse brain at all doses. (*F*–*H*) R13 improves cognitive functions in 5XFAD mice. 5XFAD mice (n = 8–10/group) orally administered control vehicle or different doses of R13 were trained in the water maze over 5 d. Shown are mean ± SEM latency to mount the escape platform (*F*), the AUC of latency (*G*), and the percentage of time spent in the target quadrant (*H*). $^*P < 0.05$ compared with vehicle-treated 5XFAD mice.

60 s. Compared with nontransgenic control mice, vehicle-treated 5XFAD mice spent a significantly lower percentage of their time in the quadrant that formerly contained the hidden platform (Fig. 5*H*), indicating severe deficits in spatial memory recall. The 5XFAD mice treated with R13 spent a significantly higher percentage of time in the target quadrant, demonstrating rescue of spatial memory. All groups of mice displayed comparable swim speeds (*SI Appendix*, Fig. S2*F*).

R13 Inhibits AEP Activation and APP and Tau Proteolytic Cleavage in 5XFAD Mice. We recently reported that delta-secretase (AEP; asparagine endopeptidase) cleaves both APP and Tau, mediating AD pathogenesis (21, 22). To explore whether R13 affects AEP's effect in AD pathologies, we conducted immunoblotting analyses, and found that mature and active AEP were dose-dependently decreased by R13, correlating with reductions in AEP-cleaved APP N373, APP N585, and Tau N368 truncates in 5XFAD mouse brains (Fig. 6*A*). To further investigate APP proteolytic cleavage activity by AEP, we conducted immunofluorescent costaining of 5XFAD brain sections with anti-APP C585 and MAP2 antibodies. With a R13 dose increase, APP C585 immunosignals were strongly inhibited by R13, inversely coupled with MAP2 augmentation (*SI Appendix*, Fig. S3*A*), indicating that R13 protects against neuronal loss. Furthermore, Tau N368 staining was also repressed by R13, coupled with the reduced pathological phosphorylation of Tau: AT-8 (*SI Appendix*, Fig. S3*B*). In agreement with these observations, IHC revealed that AEP expression in both hippocampus and frontal cortex was progressively attenuated by R13 when its dose was gradually escalated (Fig. 6 *B*–*D*). Enzymatic assays showed that AEP activity was blocked by R13 at both 21.8 and 43.6 mg/kg (Fig. 6*E*). In alignment with these observations, the inflammatory factors, including IL-1β, IL-6, and TNFα, in 5XFAD mouse brains were all repressed by R13. Thus, our data strongly support that R13 increases 7,8-DHF oral bioavailability and brain exposure and activates TrkB and its downstream signal pathways, repressing AEP and blocking APP and Tau pathological fragmentation.

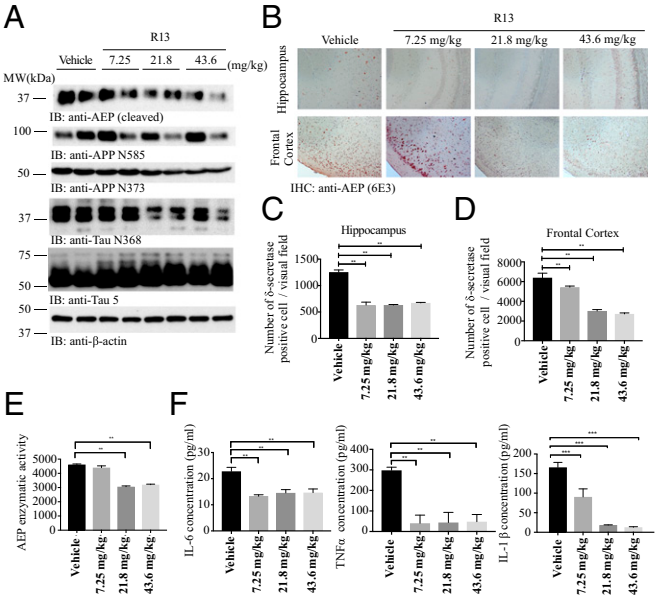

Fig. 6. R13 alleviates inflammation, inhibits AEP activation, and reduces the concentrations of AEP-derived APP fragments and Tau fragments. (*A*) Western blot showing the processing of APP and Tau by AEP. R13 significantly inhibited AEP activation by the reduction of AEP cleavage formation, which attenuated Tau and APP cleavage. (*B*) R13 repressed AEP expression in 5XFAD mice. IHC analysis showing the presence of AEP-positive cells in hippocampus and cortex of both vehicle-treated and R13-treated mice. (Scale bar: 50 μm.) (*C* and *D*) Quantitative analysis of AEP-positive cells. AEP expression in 5XFAD mice was significantly decreased by orally administered R13 at all doses. $*P < 0.01$. (*E*) AEP enzymatic activity analysis. Data are presented as mean ± SEM; $n = 5$, one-way ANOVA. $*P < 0.01$ compared with vehicle-treated mouse brains. (*F*) Proinflammatory cytokines, such as IL-1β, IL-6, and TNFα, were determined by ELISA. Chronic R13 treatment significantly decreased the IL-1β, IL-6, and TNFα production in mouse brains compared with age-related vehicle-treated mice ($n = 5$).

Discussion

In the present study, we used the prodrug strategy to improve the poor oral bioavailability of parent compound 7,8-DHF. Among the synthetic prodrugs, the carbamate prodrug R13 exhibited the most favorable in vitro and in vivo drug metabolism and PK characteristics (*SI Appendix*, Tables S1–S6). Thus, we examined in vivo PK and found that R13 exhibited ∼10.5% oral bioavailability with a C_{max} of 129 ng/mL, T_{max} of 0.5 h, and $T_{1/2}$ for oral administration of 3.66 h. Of note, 7,8-DHF plasma concentrations released from R13 (oral, 36 mg/kg) were much higher than those achieved from oral administration of higher doses of parent 7,8-DHF (50 mg/kg). The oral bioavailability for 7,8-DHF increased from 4.6% with the parent compound to 10.5% with R13 (*SI Appendix*, Table S6). As expected, TrkB receptor and its downstream p-Akt/p-MAPK signaling are potently activated on oral administration of R13, tightly correlating with 7,8-DHF concentrations in the brain (Fig. 3). The TrkB activation fits well with the in vivo PK data, supporting that the released 7,8-DHF from R13 prodrug triggers the long-lasting TrkB signaling in mouse brains.

5XFAD mice have been shown to develop cerebral amyloid plaques at 2 mo of age, and show memory impairment at 4–5 mo of age (23). It has also been shown that the level of mature BDNF is dramatically reduced in 5XFAD mice, beginning at 3 mo of age (11). Given the key roles of BDNF-TrkB signaling in learning and memory, we propose that prodrug R13 may protect memory decline in 5XFAD mice. We fed the 2-mo-old 5XFAD mice with R13 for 3 mo, and found marked activation of the TrkB receptor by 7,8-DHF in the dentate gyrus. The activation of TrkB downstream Akt and MAPK pathways are coupled to TrkB phosphorylation. Therefore, chronic oral administration of R13 activates BDNF-TrkB signaling in the brains of 5XFAD mice. Furthermore, our results are inconsistent with a previous report that systematic administration of 7,8-DHF triggers TrkB activation in a transgenic mice model of AD and in cognitively impaired aged rats (11, 24). Activation of TrkB is required for multiple aspects of neuronal function, including neuronal survival, morphological change of neurons, and synaptic plasticity (4, 25). TrkB signaling promotes the formation of dendritic spines (26). We observed a decrease in dendritic spine density in the hippocampus in 5XFAD mice, and found that R13 increased the spine density in apical dendrites of CA1 neurons of hippocampus. In agreement with these observations, R13 also exerted a rescue effect on the number of synapses in the CA1 area of the 5XFAD mode. Furthermore, the expression of synaptic markers was also increased by R13 treatment, supporting that 7,8-DHF released from R13 has a profound protective effect on synapses in vivo.

In the 5XFAD mice model, chronic oral administration of R13 activates TrkB signaling pathways in brain, attenuates synaptic loss, and reverses Aβ deposition. Consequently, R13 rescues memory deficits in 5XFAD mice. Therefore, our results suggest that 7,8-DHF released from prodrug R13 simulates the physiological actions of BDNF and prevents the synaptic dysfunction and cognitive deficits in the AD mouse model. A chronic toxicity study of R13 in C57BL6 mice involving 12 wk of consecutive treatment with daily doses of 43.6 mg/kg also showed no toxicity (*SI Appendix*, Fig. S4). Thus, these studies support that R13 is safe and

efficacious for treating AD, and is an ideal clinical candidate for drug development.

Our most recent study reveals that AEP plays a crucial role in AD and PD pathogenesis by cleaving APP, Tau, and α-synuclein (21, 22, 27). Inhibition of AEP by small molecules shows promising therapeutic efficacy in various AD mouse models (28), supporting that blockade of AEP interferes with AD progression. Here we show that TrkB activation by R13 represses AEP activation, which antagonizes APP N373, APP N585, and Tau N368 cleavage by AEP (Fig. 6), indicating that BDNF/TrkB signaling somehow mediates AEP activation. The molecular mechanisms by which the BDNF/TrkB pathway regulates AEP activation remain unknown. We recently showed that SRPK2, a cell cycle kinase activated in AD patient brains, phosphorylates AEP on S226 and activates AEP (29). Conceivably, the downstream kinases may phosphorylate AEP and inhibit its activation.

When the design of carrier-linked prodrugs is aimed at improved passive intestinal absorption, the increased lipophilicity might give rise to counterproductive physicochemical properties, such as insufficient aqueous solubility and a pronounced first-pass effect. Accordingly, R13 is less water-soluble than 7,8-DHF. Nonetheless, it effectively improves 7,8-DHF in vivo PK profiles. Special attention must be given to the metabolic differences among animal species, however; for example, rats show significantly higher rates of esterase-mediated hydrolysis than man. Therefore, PK studies in rats with esterase-activated prodrugs might overestimate the release of the active principle in man. Moreover, alkyl esters, substituted with basic moieties (e.g., tertiary amines), have not only a very short half-life in human plasma (30), but also a decreased chemical stability in buffered solutions at physiological pH. The toxicity potential of the promoiety also should be evaluated. If possible, promoieties already accepted by registration authorities or that are known to be nontoxic should be used. Metabolically labile but important pharmacophoric elements can be masked or capped to avoid rapid metabolism. For instance, in bambuterol, a prodrug of terbutaline, the phenolic groups are masked as *N*,*N*-dimethylcarbamate. The phenolic alcohol is protected from phase II metabolism, and the carbamate is slowly hydrolyzed by nonspecific cholinesterase to release the parent terbutaline. The slow metabolism results in a longer half-life. Bambuterol is dosed once daily, compared with three times daily for terbutaline (31). Conceivably, the slowly released 7,8-DHF from R13 displays much longer pharmacology than the parent compound. In summary, this study demonstrates that chronic oral administration of R13 exerts therapeutic effect in 5XFAD mice in a dose-dependent manner. R13 prodrug significantly improves 7,8-DHF oral bioavailability and increases its brain exposure. Our study supports that R13 represents a novel disease-modifying and neuroprotective pharmaceutical agent for the treatment of AD.

Materials and Methods

Mice and Reagents. 5XFAD mice were obtained from The Jackson Laboratory and were bred in a pathogen-free environment in accordance with Emory Medical School guidelines. The 5XFAD mice received vehicle or R13 dissolved in 5% DMSO/0.5% methylcellulose at a dose of 7.25, 21.8, or 43.6 mg/kg/d. Anti-TrkB antibody was purchased from Biovision. Anti–phospho-TrkB Y816 antibody was raised against [H]-CKLQNLAKASPV-pY-LDILG-[OH] (aa 806–822; EM437 and EM438) as rabbit polyclonal antibody. Anti-synaptotagmin, anti-Aβ, and anti-tubulin were purchased from Sigma-Aldrich. Anti-synapsin I, anti-PSD95, anti-spinophilin, anti-Akt, anti-p-Akt, anti-ERK, and anti–phospho-ERK1/2 antibodies were purchased from Cell Signaling Technology. Histostain-SP and Aβ 1–42 ELISA kits were purchased from Invitrogen. All chemicals not noted above were purchased from Sigma-Aldrich.

EM. Synaptic density was determined by EM as described previously (20). After induction of deep anesthesia, mice were perfused transcardially with 2% glutaraldehyde and 3% paraformaldehyde in PBS. Hippocampal slices were postfixed in cold 1% OsO_4 for 1 h. Samples were prepared and examined following standard procedures. Ultrathin sections (90 nm) were stained with uranyl acetate and lead acetate and viewed at 100 kV in a JEOL 200CX electron microscope. Synapses were identified by the presence of synaptic vesicles and postsynaptic densities.

ACKNOWLEDGMENTS. This work was supported by a grant from the National Institutes of Health (R01 DC010204, to K.Y.) and a grant from the National Natural Science Foundation of China (81771382, to Z.Z.).

1. Schliebs R, Arendt T (2006) The significance of the cholinergic system in the brain during aging and in Alzheimer's disease. *J Neural Transm (Vienna)* 113:1625–1644.
2. Corbett A, Ballard C (2012) New and emerging treatments for Alzheimer's disease. *Expert Opin Emerg Drugs* 17:147–156.
3. Giacobini E, Gold G (2013) Alzheimer disease therapy: Moving from amyloid-β to tau. *Nat Rev Neurol* 9:677–686.
4. Zuccato C, Cattaneo E (2009) Brain-derived neurotrophic factor in neurodegenerative diseases. *Nat Rev Neurol* 5:311–322.
5. Ando S, et al. (2002) Animal model of dementia induced by entorhinal synaptic damage and partial restoration of cognitive deficits by BDNF and carnitine. *J Neurosci Res* 70:519–527.
6. Nagahara AH, et al. (2009) Neuroprotective effects of brain-derived neurotrophic factor in rodent and primate models of Alzheimer's disease. *Nat Med* 15:331–337.
7. Jang SW, et al. (2010) A selective TrkB agonist with potent neurotrophic activities by 7,8-dihydroxyflavone. *Proc Natl Acad Sci USA* 107:2687–2692.
8. Choi DC, et al. (2010) Prelimbic cortical BDNF is required for memory of learned fear but not extinction or innate fear. *Proc Natl Acad Sci USA* 107:2675–2680.
9. Andero R, et al. (2011) Effect of 7,8-dihydroxyflavone, a small-molecule TrkB agonist, on emotional learning. *Am J Psychiatry* 168:163–172.
10. Liu X, et al. (2010) A synthetic 7,8-dihydroxyflavone derivative promotes neurogenesis and exhibits potent antidepressant effect. *J Med Chem* 53:8274–8286.
11. Devi L, Ohno M (2012) 7,8-dihydroxyflavone, a small-molecule TrkB agonist, reverses memory deficits and BACE1 elevation in a mouse model of Alzheimer's disease. *Neuropsychopharmacology* 37:434–444.
12. Zhang Z, et al. (2014) 7,8-dihydroxyflavone prevents synaptic loss and memory deficits in a mouse model of Alzheimer's disease. *Neuropsychopharmacology* 39:638–650.
13. Castello NA, et al. (2014) 7,8-Dihydroxyflavone, a small-molecule TrkB agonist, improves spatial memory and increases thin spine density in a mouse model of Alzheimer disease-like neuronal loss. *PLoS One* 9:e91453.
14. Chen C, et al. (2014) 7,8-dihydroxyflavone ameliorates scopolamine-induced Alzheimer-like pathologic dysfunction. *Rejuvenation Res* 17:249–254.
15. Blugeot A, et al. (2011) Vulnerability to depression: From brain neuroplasticity to identification of biomarkers. *J Neurosci* 31:12889–12899.
16. Wetsel WC, et al. (2013) Disruption of the expression of the proprotein convertase PC7 reduces BDNF production and affects learning and memory in mice. *Proc Natl Acad Sci USA* 110:17362–17367.
17. English AW, Liu K, Nicolini JM, Mulligan AM, Ye K (2013) Small-molecule trkB agonists promote axon regeneration in cut peripheral nerves. *Proc Natl Acad Sci USA* 110:16217–16222.
18. Liu X, et al. (2013) O-methylated metabolite of 7,8-dihydroxyflavone activates TrkB receptor and displays antidepressant activity. *Pharmacology* 91:185–200.
19. Shankar GM, Walsh DM (2009) Alzheimer's disease: Synaptic dysfunction and Abeta. *Mol Neurodegener* 4:48.
20. Hongpaisan J, Sun MK, Alkon DL (2011) PKC ε activation prevents synaptic loss, Aβ elevation, and cognitive deficits in Alzheimer's disease transgenic mice. *J Neurosci* 31:630–643.
21. Zhang Z, et al. (2014) Cleavage of tau by asparagine endopeptidase mediates the neurofibrillary pathology in Alzheimer's disease. *Nat Med* 20:1254–1262.
22. Zhang Z, et al. (2015) Delta-secretase cleaves amyloid precursor protein and regulates the pathogenesis in Alzheimer's disease. *Nat Commun* 6:8762.
23. Oakley H, et al. (2006) Intraneuronal beta-amyloid aggregates, neurodegeneration, and neuron loss in transgenic mice with five familial Alzheimer's disease mutations: Potential factors in amyloid plaque formation. *J Neurosci* 26:10129–10140.
24. Zeng Y, et al. (2012) 7,8-dihydroxyflavone rescues spatial memory and synaptic plasticity in cognitively impaired aged rats. *J Neurochem* 122:800–811.
25. Bekinschtein P, et al. (2008) BDNF is essential to promote persistence of long-term memory storage. *Proc Natl Acad Sci USA* 105:2711–2716.
26. Panja D, Bramham CR (2014) BDNF mechanisms in late LTP formation: A synthesis and breakdown. *Neuropharmacology* 76:664–676.
27. Zhang Z, et al. (2017) Asparagine endopeptidase cleaves α-synuclein and mediates pathologic activities in Parkinson's disease. *Nat Struct Mol Biol* 24:632–642.
28. Zhang Z, et al. (2017) Inhibition of delta-secretase improves cognitive functions in mouse models of Alzheimer's disease. *Nat Commun* 8:14740.
29. Wang ZH, et al. (2017) Delta-secretase phosphorylation by SRPK2 enhances its enzymatic activity, provoking pathogenesis in Alzheimer's disease. *Mol Cell* 67:812–825.e5.
30. Bullingham R, Monroe S, Nicholls A, Hale M (1996) Pharmacokinetics and bioavailability of mycophenolate mofetil in healthy subjects after single-dose oral and intravenous administration. *J Clin Pharmacol* 36:315–324.
31. Tunek A, Svensson LA (1988) Bambuterol, a carbamate ester prodrug of terbutaline, as inhibitor of cholinesterases in human blood. *Drug Metab Dispos* 16:759–764.